Mechanism of the transition from fractal to dendritic growth of surface aggregates

Harald Brune, Christoph Romainczyk, Holger Röder & Klaus Kern

Institut de Physique Expérimentale,
Ecole Polytechnique Federal de Lausanne, CH-1015 Lausanne, Switzerland

THE similarity of many patterns formed in non-equilibrium growth processes in physics, chemistry and biology is conspicuous, and many attempts have been made to discover common mechanisms underlying their formation[1]. A central question is what causes some patterns to be dendritic (symmetrically branched, like snowflakes) and others fractal (randomly ramified). In general, the transition from fractal to dendritic growth is regarded as a manifestation of the predominance of anisotropy over random noise in the growth process. In electrochemical deposition, this transition is observed as the growth speed is varied[2,3]. Here we report a crossover from fractal to dendritic growth in two dimensions on the microscopic scale. We use the scanning tunnelling microscope to study diffusion-limited aggregation of silver atoms on a Pt(111) surface. The transition occurs as the deposition flux is increased, and our observations suggest that the increasing importance of anisotropy of edge diffusion at higher flux is responsible for this crossover. We anticipate that a similar phenomenon may operate in three-dimensional crystal growth.

The direct experimental analogue to the two-dimensional diffusion limited aggregation (DLA) simulations[4,5] is vapour-phase epitaxy of metals on single-crystal metal surfaces at low temperatures. The film atoms, once adsorbed on the surface from the gas phase, diffuse in a random walk until they stick irreversibly to the perimeter of a growing aggregate. If perimeter diffusion is prohibited or is negligibly small, classical fractals result[6]. If a certain perimeter mobility is allowed and this mobility is anisotropic, however, deviations from this behaviour can occur, as will be demonstrated here.

In our experiments the parameters controlling growth are the temperature and flux of deposition, the former determining the perimeter mobility and the latter the growth velocity. The experiments were performed in ultra-high vacuum with standard facilities for sample preparation and film evaporation. We applied variable-temperature scanning tunnelling microscopy (STM)[7] to image the Ag cluster morphology isotherm to deposition because the patterns formed are metastable. In the STM images the derivative $\partial z/\partial x$ of the lines of constant tunnel current has been

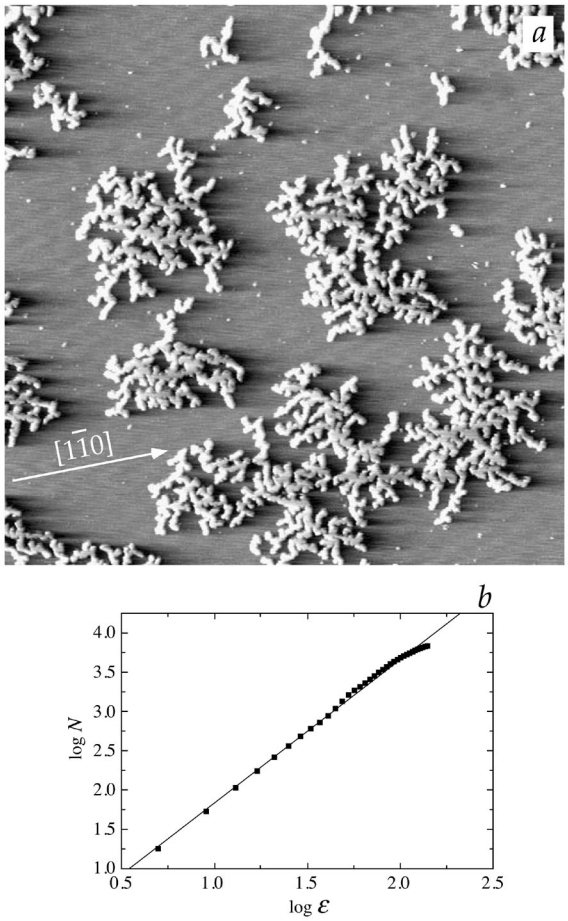

FIG. 1 *a*, STM image showing fractal Ag aggregates grown on Pt(111) at 110 K and a deposition flux (R) of 1.6×10^{-5} monolayers per second; one monolayer (ML) corresponds to the density of the Pt(111) substrate of 1.50×10^{15} atoms cm^{-2} (size, 1,200 Å × 1,200 Å; coverage θ = 0.12 ML). *b*, Ag cluster (lower right in *a*) obeys a fractal dimension of $D = 1.78$ for the straight line fitted to the data; ε is the border length of boxes in pixel (1 pixel corresponds to 2.3 Å^2), N is the number of pixels where the surface is covered by Ag.

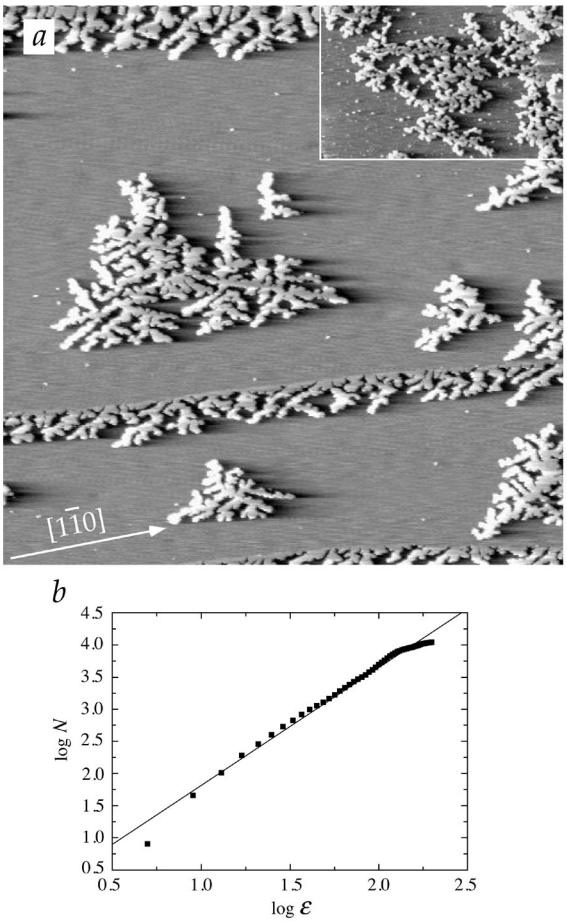

FIG. 2 *a*, STM image showing the dendritic shape of the Ag aggregates grown at 130 K with a flux (R) of 1.1×10^{-3} ML s^{-1} (1,200 × 1,200 Å, $\theta=0.12$ ML), note also that two Pt substrate steps are crossing the image almost horizontally. *b*, Mass–length scaling of the biggest dendrite in *a*. Inset in *a*, Transition from the dendritic to fractal growth at 130 K on lowering the deposition flux by two orders of magnitude (830 × 520 Å, $\theta=0.12$ ML, $R=1.6\times10^{-5}$ ML s^{-1}).

recorded. They therefore represent the surface as it appears when illuminated from the left.

The two-dimensional Ag aggregates shown in Fig. 1*a* have been grown at 110 K at a low Ag flux. Large clusters (~3,000 atoms) with an open ramified structure are formed under these conditions. The branches of the clusters frequently alter their direction of growth and thus show no long range correlation with the trigonal substrate symmetry. The branches are of monoatomic height, their thickness is almost constant over the entire aggregate and much smaller than its radius of gyration. In fact the arms are only 2 ± 1 atoms wide as determined from the total arm length and the cluster size. The shape of the Ag aggregates grown at 110 K is very similar to that of fractal aggregates simulated with the classical DLA computer codes either performed off-lattice (no anisotropy)[5,8] or on-lattice with noise dominating lattice anisotropy[4,5].

In order to examine the fractal character of the Ag aggregates shown in Fig. 1*a* we have determined their fractal dimension D. For that purpose we arranged boxes with border length ε centred at the centre of mass of the aggregate and counted the number of pixels N with grey levels corresponding to Ag as a function of box size ε (ref. 1). $N(\varepsilon)$ is shown in Fig. 1*b* for the large Ag cluster located on the lower right-hand side of Fig. 1*a*. It is evident that the number of Ag-covered pixels N scales over two orders of magnitude with the box size as ε^D, where $D=1.78$. The scaling is limited at small lengths by the finite apparent branch width of 14 Å (partly due to curvature of the STM tip) and at large lengths by the finite cluster size. By investigating the variation of mass with size of numerous Ag aggregates grown at 110 K, we find the average fractal dimension to be $D=1.76\pm0.07$. This experimental value is in good agreement with two-dimensional DLA simulations[4,5].

A drastic change of the aggregate patterns is observed when the flux is increased by two orders of magnitude. Figure 2*a* demonstrates that Ag clusters grown with this higher growth speed obey a nice dendritic pattern. It shows the characteristic 'back-bones', whose orientation is determined by the crystalline anisotropy of the substrate. In snow-flake terminology this dendrite is of the P2a type (plane P, with irregular number of branches 2, three branched a). Although the qualitative growth form has changed dramatically, the fractal dimension is almost unaffected. From the mass–length scaling plot in Fig. 2*b* we infer a fractal dimension of $D=1.77\pm0.05$ for the biggest cluster in Fig. 2*a*, which agrees with that of the randomly ramified aggregates of Fig. 1*a*. This is expected from DLA for the relatively small cluster sizes under consideration here[9].

It is important to notice that the slight increase in temperature to 130 K chosen for Fig. 2*a* (in order to obtain clusters with comparable size to those in Fig. 1*a*) has no influence on the cluster shape. The inset in Fig. 2*a* shows that randomly ramified patterns (with no preferred orientation) result at 130 K through application of the low flux. On the other hand, dendrites also grow at 110 K upon deposition with the high flux used in Fig. 2*a* (not shown here). Therefore the parameter that drives the crossover from ramified to dendritic patterns is the deposition flux, that is, the growth speed of the aggregate.

These observations are in agreement with earlier work on other systems. Increasing the growth speed (Zn^{2+} concentration

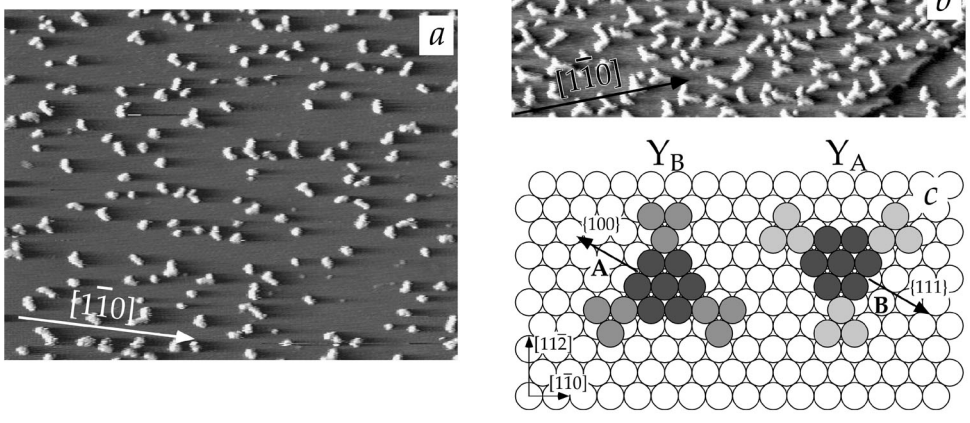

FIG. 3 *a*, *b*, STM images of small Ag_n clusters grown on Pt(111) at 80 K with an average cluster size of $n=13$ in *a* and $n=21$ atoms in *b* respectively; (*a*; 600 × 470 Å, $\theta=0.037$ ML, $R=3.7\times10^{-4}$ ML s^{-1}. *b*, 600 × 190 Å, $\theta=0.12$ ML, $R=3.6\times10^{-3}$ ML s^{-1}). *c*, Schematic model showing the two possible Y-shaped cluster orientations.

and voltage) in electrochemical deposition resulted in transition from fractal to dendritic patterns[2,3]. In fluid systems (Saffman–Taylor instability in the propagation of a low-viscosity medium into one of a high viscosity) dendrites have been found for high pressures and anisotropy whereas low expansion rates produced fractals[10–12]. Side branching, the necessary condition for dendrites, can also be obtained by the presence of a bubble at the interface tip that prevents its splitting and increases its propagation speed[13]. The hydrodynamic experiments were simulated with a statistical mechanic approach that demonstrated the importance of anisotropy for dendritic growth[14,15]. Similarly in DLA work, this transition from fractal to dendritic patterns is obtained when anisotropy dominates noise[8,16–18]. The microscopic mechanism that establishes anisotropy only at increased growth rates to the macroscopic pattern shape, however, can be analysed for the present system.

From a comparison with DLA studies, it is found that the anisotropy that characterizes dendrites here comprises preferential growth in only three of the six $\langle 112 \rangle$ directions[9]. The nature of this anisotropy for growth of Ag on Pt(111) is linked to the trigonal symmetry of this surface. A densely packed cluster on a face-centred cubic (111) surface is bound by two types of edges with atomically different structures (A and B edges): A edges are $\{100\}$ facets whereas B edges are $\{111\}$ facets (Fig. 3*c*). This microscopic difference is partly reflected in a different activation barrier for perimeter diffusion. To identify which of the close-packed Ag-edge orientations is of A-type and which is of B-type, it is important to note that the Ag atoms reside on f.c.c. sites on the Pt(111) surface for coverages of up to a monolayer. This site can be deduced from the perfect (dislocation-free) attachment of Ag islands to the neighbouring Pt layer at ascending steps (stacking faults would produce undulations in the STM images[19], but none is evident in the figures—for example, the Ag islands are flat at the step edges in Fig. 2*a*). For Ag on Pt(111), our investigations (analogous to those of Michely *et al.*[20]) show that diffusion along B steps is faster than along A steps below 200 K, and thus that the former has a lower activation barrier. Interestingly, this is the reverse of what is found for homoepitaxial systems[21].

This kinetic difference is especially pronounced at low temperature. Figure 3*a* and *b* shows the initial branching of the cluster seed at 80 K. The smaller islands that appear almost spherical in Fig. 3*a* are heptamers, and constitute the seed particle. The biggest islands are forming Y's with arms 120° apart. Y-branching of the heptamer is possible in two ways: by adding Ag adatoms to its A-steps or to its B-steps (see left- and right-hand side of Fig. 3*c*). In our experiment we only observe the Y_A-cluster. This anisotropy in growth is even better seen for somewhat bigger clusters as shown in Fig. 3*b* (note the different orientation of the crystallographic $[1\bar{1}0]$ direction compared to Fig. 3*a*). The branches of the Y_As are exactly in the preferred growth directions found for the bigger dendrite at 130 K. Because Ag atoms arrive at random at each edge orientation, the fact that we find only the Y_A type must involve perimeter diffusion along B-steps, whereas diffusion along A-steps is frozen in. There is, however, a second necessary condition for the observed growth of Y_As, that applies after the addition of the first three atoms to the heptamer (which is most plausibly done at A-steps): the Ag_{10} aggregate is then exclusively bound by B-steps. In order to grow a stable expansion in the A-direction, as observed, two diffusing perimeter atoms have to meet each other at the aggregate's corners.

Such an event, however, is the more probable the more diffusing atoms similarly are present at the island perimeter. Their quantity is directly related to the flux. At the high flux used in Fig. 2*a* there are on the average 100 atoms arriving per second at the aggregate's perimeter, whereas there is only one per second at the low flux of Fig. 1*a*. In addition, the mean free path of a diffusing perimeter atom increases only with square root of the diffusion time (one-dimensional random walk). Therefore the probability for two atoms to meet at a corner is greater at increased flux, and, due to faster migration along B-steps, much greater at those corners that point in the A-direction. Thus dendrites with trigonal growth perpendicular to A-steps are formed for high flux. At low flux, on the other hand, interaction of two diffusing particles at the island corner is much less probable, and predominantly single non-interacting mobile atoms are present at the step. Anisotropy therefore loses its importance in favour of noise, and the aggregate grows randomly. □

Received 30 December 1993; accepted 31 March 1994.

1. Takayasu, H. *Fractals in the Physical Sciences* (Manchester Univ. Press, New York, 1990).
2. Sawada, Y., Dougherty, A. & Gollub, J. P. *Phys. Rev. Lett.* **56,** 1260–1263 (1986).
3. Grier, D., Ben-Jacob, E., Clarke, R. & Sander, L. M. *Phys. Rev. Lett.* **56,** 1264–1267 (1986).
4. Witten, T. A. & Sander, L. M. *Phys. Rev. Lett.* **47,** 1400–1403 (1981).
5. Meakin, P. *Phys. Rev.* A**27,** 1495–1507 (1983).
6. Hwang, R. Q., Schröder, J., Günther, C. & Behm, R. J. *Phys. Rev. Lett.* **67,** 3279–3282 (1991).
7. Röder, H., Hahn, E., Brune, H., Bucher, J. P. & Kern, K. *Nature* **366,** 141–143 (1993).
8. Eckmann, J. P., Meakin, P., Procaccia, I. & Zeitak, R. *Phys. Rev. Lett.* **65,** 52–55 (1990).
9. Meakin, P. *Phys. Rev.* A**33,** 3371–3382 (1986).
10. Ben-Jacob, E., *et al. Phys. Rev. Lett.* **55,** 1315–1318 (1985).
11. Buka, A., Kertész, J. & Vicsek, T. *Nature* **323,** 424–425 (1986).
12. Horváth, V., Vicsek, T. & Kertész, J. *Phys. Rev.* A**35,** 2353–2356 (1987).
13. Couder, Y., Cardoso, O., Dupuy, D., Tavernier, P. & Thom, W. *Europhys. Lett.* **2,** 437–443 (1986).
14. Nittmann, J. & Stanley, H. E. *Nature* **321,** 663–668 (1986).
15. Nittmann, J. & Stanley, H. E. *J. Phys. A* **20,** L1185–L1191 (1987).
16. Meakin, P. *Phys. Rev.* A**36,** 332–339 (1987).
17. Vicsek, T. *Fractal Growth Phenomena* (World Scientific, Singapore, 1989).
18. Eckmann, J. P., Meakin, P., Procaccia, I. & Zeitak, R. *Phys. Rev.* A**39,** 3185–3195 (1989).
19. Brune, H., Röder, H., Boragno, C. & Kern, K. *Phys. Rev.* B**49,** 2997 (1994).
20. Michely, T., Hohage, M., Bott, M. & Comsa, G. *Phys. Rev. Lett.* **70,** 3943–3946 (1993).
21. Ehrlich, G. *Surf. Sci.* **246,** 1–12 (1991).

ACKNOWLEDGEMENTS. This work was supported by the Schweizerische Nationalfonds.